

Plasmonic, Low-Frequency Raman, and Nonlinear Optical-Limiting Studies in Copper–Silica Nanocomposites

Satyabrata Mohapatra · Y. K. Mishra · A. M. Warriar ·
Reji Philip · S. Sahoo · A. K. Arora · D. K. Avasthi

Received: 12 May 2011 / Accepted: 28 July 2011 / Published online: 4 August 2011
© Springer Science+Business Media, LLC 2011

Abstract Nanocomposite thin films consisting of Cu nanoparticles embedded in silica matrix were synthesized by atom beam co-sputtering technique. Plasmonic, optical, and structural properties of the nanocomposite films were investigated by using ultraviolet (UV)–visible absorption spectroscopy, nonlinear optical transmission, X-ray diffraction (XRD), and low-frequency Raman scattering. UV–visible absorption studies revealed the surface plasmon resonance absorption at 564 nm which showed a red shift with increase in Cu fraction. XRD results together with surface plasmon resonance absorption confirmed the presence

of Cu nanoparticles of different size. Low-frequency Raman studies of nanocomposite films revealed breathing modes in Cu nanoparticles. Nanocomposites with lower metal fractions were found to behave like optical limiters. The possibility of controllably tuning the optical nonlinearity of these nanocomposites could enable them to be the potential candidates for applications in nanophotonics.

Keywords Plasmonic nanocomposites · Nonlinear absorption · Optical limiting · Surface plasmon resonance

S. Mohapatra (✉)
School of Basic and Applied Sciences,
Guru Gobind Singh Indraprastha University,
Dwarka, New Delhi 110075, India
e-mail: smiuac@gmail.com

Y. K. Mishra
Functional Nanomaterials, Institute for Materials Science,
University of Kiel,
Kaiserstrasse 2,
24143 Kiel, Germany

A. M. Warriar · R. Philip
Light and Matter Physics Group, Raman Research Institute,
C.V. Raman Avenue, Sadashivanagar,
Bangalore 560 080, India

S. Sahoo · A. K. Arora
Condensed Matter Physics Division,
Indira Gandhi Centre for Atomic Research,
Kalpakkam, Tamil Nadu 603102, India

D. K. Avasthi
Inter University Accelerator Centre,
Post Box–10502, New Delhi 110067, India

Introduction

Noble metal nanoparticles (MNPs) embedded in a dielectric matrix have attracted significant research interest due to their fascinating optical, electrical, and mechanical properties, which find a wide range of applications in nano- to biotechnology [1–8]. When noble MNPs embedded in a dielectric matrix are excited by light, the electric field vector of the electromagnetic (EM) wave induces charge density oscillations called plasmon oscillations. When the frequency of EM wave equals to the plasmon oscillation frequency, i.e., under resonance condition, strong absorption of light occurs, which is known as localized surface plasmon resonance (LSPR) absorption. LSPR phenomenon in metal nanoparticles (NPs) under EM radiation results in strong enhancement of local electric fields by orders of magnitude, which in turn leads to significant enhancement in their linear and nonlinear optical properties [9–12]. Due to this, nanocomposites embedded with noble metal nanoparticles find widespread applications in chemical and biosensors, surface-enhanced Raman scattering, sub-wavelength lithography, and nonlinear optical devices

[13–21]. The optical nonlinearity and optical-limiting phenomena in noble metal dielectric nanocomposites are promising for potential applications in photonics, optoelectronics, waveguides, and lasers. The plasmonic or optical properties of noble metal dielectric nanocomposites mainly depend on the type of matrix, size and shape of NPs, and inter-particle separation (IPS) which is mainly responsible for coupling of electric field when IPS is below a threshold value [22, 23]. In nanoscale region (1 to 10 nm), the surface contribution strongly dominates over bulk properties and the phenomenon like inter- and intraband contributions also come into picture along with plasmon oscillations in the noble MNPs under EM excitation. Therefore, a detailed understanding of their optical properties is of interest from both fundamental as well as technological point of view. Development of techniques for synthesizing monodisperse MNPs with desired sizes and IPS has been a major challenge over the years. Several techniques [23–29] have been used to fabricate MNPs embedded in various dielectric matrices. In this paper, we report the synthesis of Cu–silica nanocomposite thin films by a simple and versatile process of atom beam co-sputtering. The effects of metal fraction on the surface plasmon resonance (SPR) absorption and the nonlinear optical properties of nanocomposites are investigated. Size-dependent, low-frequency, Raman-breathing modes in Cu nanoparticles have been investigated and optical-limiting response is also reported.

Experimental Details

Nanocomposite films of Cu–silica (marked as a, b, and c) with increasing concentration of Cu were prepared by atom beam co-sputtering of Cu and silica targets with 1.5 keV neutral Ar atoms. Cu thin foils symmetrically glued (in square pieces) on 3-in. diameter silica disc was used as sputtering target. The FAB neutral Ar atom source is mounted at an angle of 45° to the sputter target and the distance between source and target was adjusted in such a manner that the beam covers the entire area of target. The circular substrate holder with diameter slightly less than 3 in. was mounted exactly below the target so that the whole area of target receives maximum yield of sputtered atoms from the target. The relative areas of Cu foils and silica disc, exposed to the Ar atom beam, and the sputtering yields were taken into consideration for deciding the metal content of the nanocomposite films. The uniformity of the co-sputtered films was achieved by rotating the substrate with a DC motor. Films deposited on silica glass were used for ultraviolet (UV)–visible optical absorption, z-scan, and low-frequency Raman scattering studies, while films on Si (100) substrates were used for X-ray diffraction (XRD) and

Rutherford backscattering spectroscopy (RBS) investigations. RBS using 900 keV He⁺ ions at a backscattering angle of 165° was used to quantify the Cu concentration and thickness of the nanocomposite films. UV–visible absorption spectra were recorded using a dual beam spectrophotometer Hitachi U3300 in the spectral range of 300–800 nm. Grazing incidence X-ray diffraction spectra were recorded by Bruker D8 Advance diffractometer at grazing incidence angle of 2°, using a CuK_α ($\lambda=1.5406 \text{ \AA}$) source operating at 40 kV and 40 mA. Low-frequency Raman scattering (LFRS) studies at room temperature in the backscattering geometry were carried out using Spex-14018 monochromator and 488 nm line of an Ar ion laser was used as excitation source. To study optical nonlinearity, open aperture z-scan measurements were carried out at 532 nm using 7-ns laser pulses from a frequency-doubled Nd:YAG laser (Quanta Ray-Spectra Physics). The z-scan is a widely used technique developed by Bahae et al. [30] to measure optical nonlinearity of materials and the open aperture z-scan gives information about the nonlinear absorption coefficient. Here, a laser beam is focused using a lens and passed through the sample. The beam's propagation direction is taken as the z-axis, and the focal point is taken as $z=0$. The beam will have maximum energy density at the focus, which will symmetrically reduce towards either side for the positive and negative values of z . The experiment is done by placing the sample in the beam at different positions with respect to the focus (different values of z) and measuring the corresponding light transmission. The graph plotted between the sample position z and the normalized transmittance of the sample T (norm.) (transmission normalized to the linear transmission of the sample) is known as the z-scan curve. The nonlinear absorption coefficient of the sample can be numerically calculated from the z-scan curve. In our experiment, z-scans were recorded at three different laser pulse energies (18, 22, and 33 μJ) to ensure reproducibility of the results. The beam focal spot radius (ω_0) was 18 μm , yielding a Rayleigh range (z_0) of 1.9 mm. The laser was run in the single shot mode using a data acquisition program, with an approximate interval of 2 to 3 s between each pulse. This low repetition rate prevents sample damage and heating of the sample during the z-scan.

Results and Discussions

Figure 1 shows a typical RBS spectrum of Cu–silica nanocomposite (sample a) deposited on Si substrate, along with the simulated spectrum. The Cu content and thickness of the nanocomposite film have been estimated to be 18 ± 1 at.% and 130 nm respectively from Rutherford universal manipulation program simulations [31]. The Cu contents of

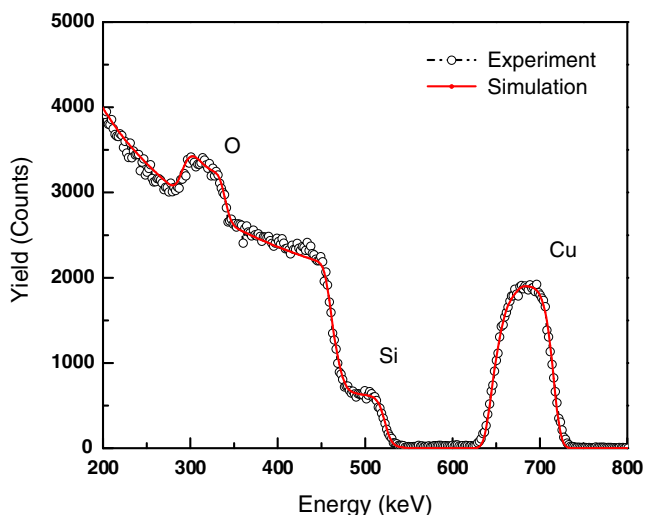


Fig. 1 A typical RBS spectrum of Cu–silica nanocomposite (a) along with the simulated spectrum, shown by continuous red line

nanocomposites b and c have been found to be 35 ± 2 and 63 ± 3 at.%, respectively.

The optical absorption spectra of Cu–silica nanocomposites (a, b, and c) with increasing Cu metal-filling fractions are shown in Fig. 2. The spectrum for sample a shows the presence of a broad-absorption band at ~ 561 nm (inset of Fig. 2), which is due to the SPR absorption of Cu NPs embedded in silica matrix. The increased absorption in the UV region is mainly due to the interband contributions. The absorbance for sample b shows a prominent SPR peak at 564 nm. Further increase in Cu metal fraction of the nanocomposite films (sample c) results in a significant increase in the intensity of SPR peak which is red shifted to ~ 579 nm along with slight increase in full width at half

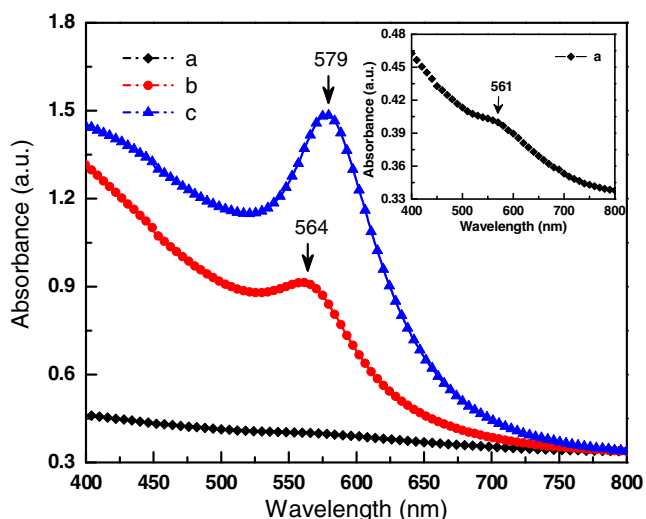


Fig. 2 UV–visible absorption spectra of Cu–silica nanocomposites (a, b, and c) having different metal fractions

maximum (FWHM). The observed red shift, broadening, and increased intensity of the SPR peak are attributed to increase in size and density of embedded Cu NPs in the nanocomposites [9]. In addition, the IPS becomes comparable or smaller than the size of Cu NPs leading strong coupling of plasmons which again results in the creation of strong local electric fields, and hence enhanced absorption of electromagnetic radiation. This can be clearly seen in the spectrum for sample c, in which the IPS is estimated to be smaller due to higher Cu content of the nanocomposite.

The XRD spectra of the nanocomposite films (a, b, and c) are shown in Fig. 3, which reveal that embedded Cu NPs are in face-centered cubic phase. The broad peaks in XRD pattern reflect the finite size of Cu NPs. The most intense peak (at 43.1°) in XRD pattern is due to the reflection from (111) plane and the broad peak around 50.3° is due to the (200) reflection from Cu NPs. The appearance of an additional peak at $\sim 35.5^\circ$ in XRD spectra can also be seen for samples b and c, which can be attributed to (–111) the reflection of CuO. It can also be clearly seen from Fig. 3 that the FWHM of the (111) peaks in the XRD spectra decreases with increase in the Cu content of nanocomposites, which indicates the increase in the average size of embedded Cu NPs.

LFRS is commonly used to determine the size of NPs embedded in dielectric matrices. The confined acoustic phonons in metal or semiconductor NPs give rise to low-frequency (few cm^{-1} to few tens of cm^{-1}) modes in the vibrational spectrum. The energy eigenvalues of these vibrational modes mainly depend on the elastic properties (longitudinal and transverse sound velocities) of the material and the size of NPs. These modes are characterized by two indices l and n , where l is the angular momentum quantum number and n is the branch number. Here, $n=0$

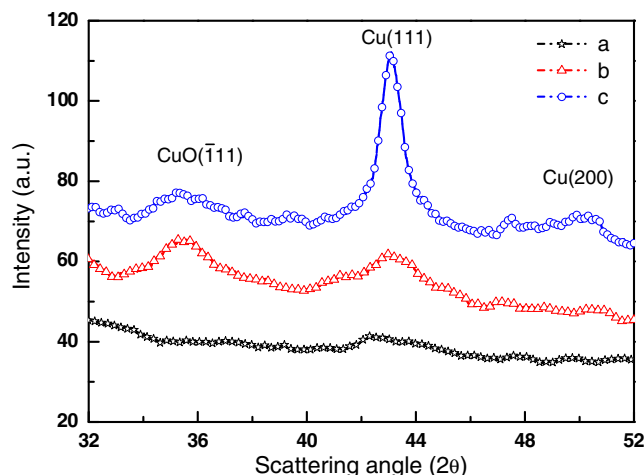


Fig. 3 XRD spectra of Cu–silica nanocomposites (a, b, and c) having different metal fractions

represents the surface modes. It has been verified both theoretically and experimentally that only two types of acoustic vibration modes are Raman active. These are the symmetric surface spheroidal mode (breathing mode) corresponding to $l=0$ and the asymmetric surface quadrupolar mode corresponding to $l=2$. The frequencies of the spheroidal mode (breathing mode) ω_0 and the quadrupolar mode ω_2 are given as [32]:

$$\omega_0 = A_0 \frac{V_L}{d c} \quad (1)$$

$$\omega_2 = A_2 \frac{V_T}{d c} \quad (2)$$

where ω_0 and ω_2 are the frequencies of the vibration modes with $l=0$ and $l=2$, v_L and v_T are the longitudinal and transversal sound velocities, A_0 and A_2 are proportionality coefficients depending on the angular momentum l , the harmonic number n , and the ratio between the longitudinal and transverse sound velocities, c is the velocity of light in vacuum, and d is the diameter of the NPs. Since the frequency is inversely proportional to the size of the

particles, small NPs would result in LFRS peaks at relatively higher wave numbers, which are weak in intensity and very difficult to detect. Nanoparticles of larger size gives rise to LFRS peaks, at very low wave numbers, submerged with the Rayleigh peak. However, it is possible to detect LFRS peaks lying in the range of 5 to 40 cm^{-1} which corresponds to particles which are few nanometers in size. Hence, LFRS can be used to determine the size of small metal or semiconductor NPs embedded in dielectric matrices.

LFRS was used to determine the size of Cu NPs embedded in silica matrix. Montagna and Dusi [33] have calculated the values of coefficients A_0 and A_2 as a function of v_L/v_T . The value of A_0 comes out to be 0.83 using their calculation and the reported values of sound velocities for bulk copper $v_L=4,828$ m/s and $v_T=2,648$ m/s. We have estimated the size (diameter) of Cu NPs from the observed frequencies of the low-frequency Raman peaks using these parameters from Eq. (1). The low-frequency Raman spectra of Cu–silica NC films with different Cu metal-filling fractions (samples a, b, and c) are shown in Fig. 4. The observed peaks have the following frequencies: 24 cm^{-1}

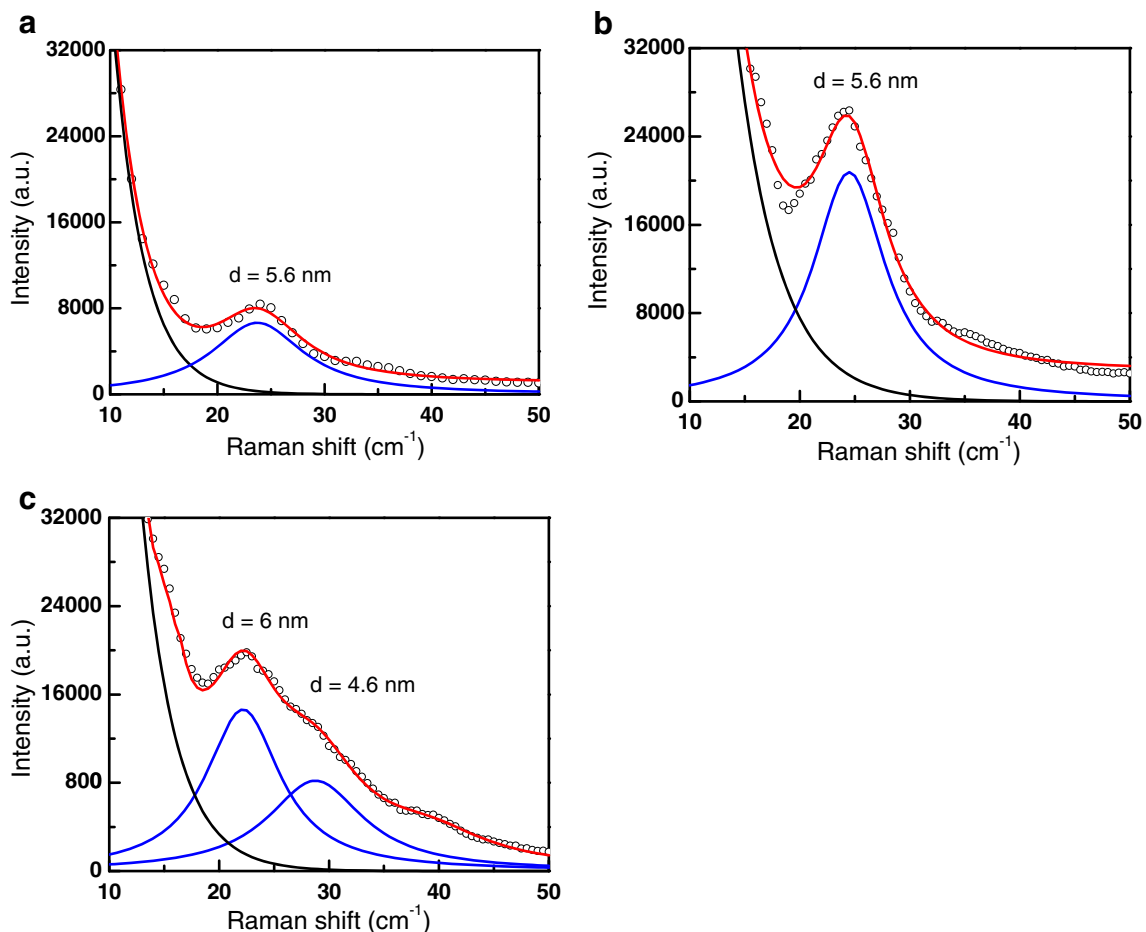


Fig. 4 Low-frequency Raman spectra for Cu–silica nanocomposites (a, b, c) having different metal fractions

(5.6 nm) for sample a, 24.2 cm^{-1} (5.6 nm) for sample b, and 22.2 cm^{-1} (6 nm) and 28.9 cm^{-1} (4.6 nm) in case of sample c. The values in the brackets are the corresponding average diameters of Cu NPs, estimated assuming the observed Raman peaks originated from the spheroidal “breathing mode” ($l=0$) of Cu NPs.

The formation and growth of Cu NPs inside silica matrix by atom beam co-sputtering can be explained as follows. Nanoparticle formation inside an insulating matrix by atom beam co-sputtering involves processes of (a) surface and bulk diffusion of sputter-deposited atoms, (b) nucleation and growth of nanoparticles, and (c) adsorption and desorption of atoms from these nanoparticles. In the present case, 1.5 keV Ar atoms have been used to sputter silica target with some area covered homogenously with thin Cu foils. Irradiation with 1.5 keV Ar atoms leads to the sputtering of O, Si, and Cu atoms with energies varying from few electron volt to hundreds of electron volt, as estimated using stopping and range of ions in matter (SRIM) code [34]. These sputtered atoms get deposited on the substrates leading to the formation of thin films, which gets continually irradiated with the energetic sputtered atoms. The projected range and range straggling of these sputtered atoms are estimated to be in the range of few angstrom from SRIM simulations [34]. These atoms diffuse on surface and into the matrix because of their remaining energy. Due to the very low solubility of Cu in silica matrix, the diffusing Cu atoms combine to form clusters which then act as nucleation centers for the growth of Cu NPs. The nucleation and growth of Cu NPs depends on average interatomic separation of Cu atoms arriving in the film, which is dependent on the Cu content of the nanocomposite films. The size of Cu NPs formed depends on the Cu content of the films and the energies of the sputtered atoms irradiating the films during its growth. An increase in Cu content results in the growth of Cu NPs with increased number density.

Figure 5a shows the open aperture z-scan curve giving the nonlinear transmittance of the Cu–silica nanocomposite sample a. In Fig. 5b, we show the normalized transmittance as a function of the input laser intensity. Since we are using nanosecond laser pulses for excitation, there is a possibility for photobleaching and sample melting. These will lead to the loss of symmetry of the z-scan about the $z=0$ point, and an increased light scattering when the sample is at and near the beam focal point. However, the z-scans shown in Fig. 5a are symmetric. Moreover, we had visually checked for increased light scattering from the samples throughout the z-scan, but did not observe any. These observations indicate that the sample has undergone no physical or chemical changes due to laser excitation. At the excitation energy used an optical-limiting behavior is clearly seen for

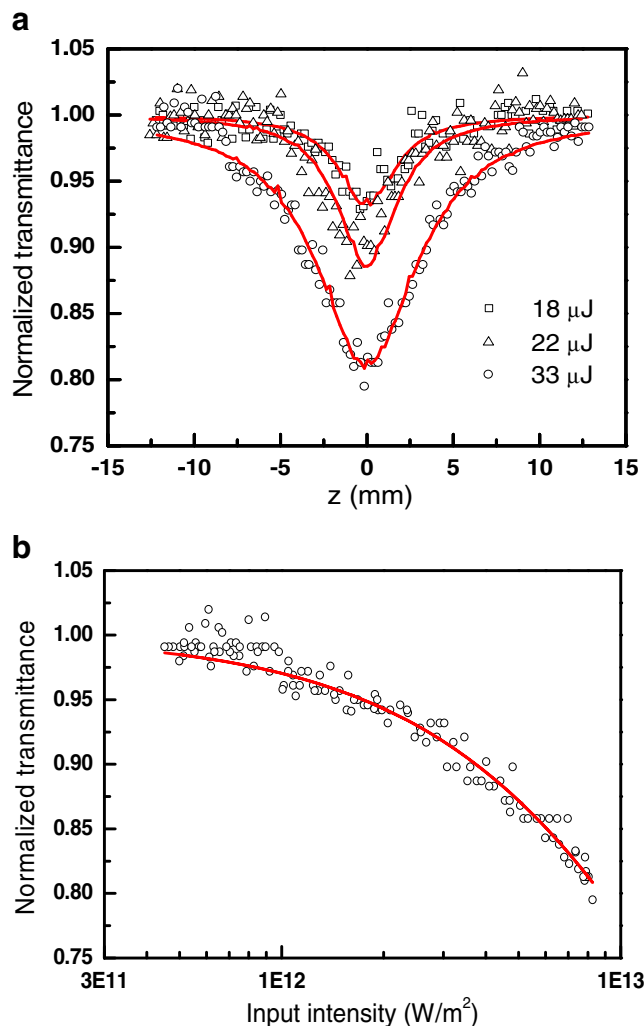


Fig. 5 (a) Open aperture z-scan plots of Cu–silica nanocomposite film a and (b) normalized transmittance as a function of input laser intensity. *Open symbols* are the measured data points while *solid curves* are numerical fits to the data for a two-photon absorption process given by Eq. 3

the nanocomposite with lowest Cu content (at lower energies an absorption saturation behavior may be expected in noble metal nanoparticle systems). For sample a, which behaves like an optical limiter, the nonlinearity is found to fit well to the transmission equation for a two-photon type absorption (2PA) process, given by [35]

$$T = \left(\frac{(1 - R)^2 \exp(-\alpha L)}{\sqrt{\pi q_0}} \right) \int_{-\infty}^{\infty} \ln \left[\sqrt{1 + q_0 \exp(-t^2)} \right] dt \tag{3}$$

where T is the actual z -dependent sample transmission (product of linear transmission and normalized transmittance), and L and R are the length and surface reflectivity of the sample, respectively. α is the linear absorption coefficient. q_0 is given by $\beta(1 - R)I_0L_{eff}$, where β is the

nonlinear absorption coefficient, and I_0 is the on-axis peak intensity. L_{eff} is given by $1 - \exp(-\alpha L/\alpha)$. Since the residual absorption of sample a at the excitation wavelength is 61%, the quantity β here is derived not only from genuine 2PA, but also from interband, intraband, and free carrier absorptions. Collectively, these phenomena act as a reverse saturable absorption process, and β may therefore be called the effective 2PA coefficient. The effective β values are calculated to be 2×10^{-7} , 3×10^{-7} , and 6×10^{-7} m/W for the excitation energies of 18, 22, and 33 μ J, respectively. The observed values of nonlinear absorption coefficient β have been compared to the results reported earlier for different nanocomposites. Under similar excitation conditions, we have measured the effective β values of ZnMgO thin films in the range of 10^{-5} m/W [36], PbSrTiO₃ films in the range of 10^{-7} m/W [37], while for Au: Ag-PVA, Ag-PVA, and Au-PVA nanocomposite films, these values were measured in the range of 10^{-7} , 10^{-8} , and 10^{-9} m/W, respectively [38]. Irimpan et al. [39] have shown that the effective β values of ZnO–Ag nanocomposite can be tuned from 2×10^{-10} to 2×10^{-9} m/W by increasing the Ag metal fraction. Kartikeyan et al. [26] have reported effective β values in the range of 5×10^{-12} to 10^{-10} m/W for ion-exchanged Cu nanocomposite glass. Takeda et al. [25] have measured β of Cu-implanted silica glass nanocomposites in the range of 10^{-8} to 10^{-9} m/W. The observed effective β values are orders of magnitude larger as compared to the values reported for Cu–silica nanocomposites, prepared by other methods. Thus, the nonlinear absorption coefficient measured by z-scan technique reveals that the Cu–silica nanocomposites investigated in the present study have good nonlinear optical response and could be chosen as ideal candidates with potential applications in nonlinear optics and photonics.

Conclusion

In summary, we have synthesized Cu–silica nanocomposite thin films with various Cu concentrations by a simple process of atom beam co-sputtering of Cu and silica. UV–visible studies revealed a clear SPR absorption band of Cu nanoparticles which showed red shift of ~ 18 nm with increase in Cu metal fraction. X-ray diffraction together with low-frequency Raman scattering studies confirmed the growth of Cu nanoparticles with an increase in Cu metal fraction. The nucleation and growth of Cu nanoparticles in silica during co-sputtering process have been discussed. Nonlinear optical properties of nanocomposite films are investigated in detail and we demonstrate that Cu–silica nanocomposite with Cu metal fraction ~ 18 at.% behaves like an optical limiter. Since optical limiters have several applications in lasers and optoelectronics, Cu–silica nano-

composite films can be potential media for photonics applications.

Acknowledgments The authors are thankful to S. R. Abhilash for his help during sample preparation. SM is grateful to Department of Science and Technology, New Delhi for providing financial support under SERC Fast Track Young Scientist project. The authors are grateful to Prof. H. Hofsäss for fruitful discussion and RBS measurements. YKM acknowledges the Alexander von Humboldt Foundation, Bonn, Germany for Humboldt Research Fellowship.

References

1. Kano H, Kawata S (1996) Two-photon-excited fluorescence enhanced by a surface plasmon. *Opt Lett* 21:1848
2. Beecroft LL, Ober CK (1997) Nanocomposite materials for optical applications. *Chem Mater* 9:1302
3. Nie S, Emory SR (1997) Probing single molecules and single nanoparticles by surface-enhanced Raman scattering. *Science* 275:1102
4. Bhawalkar D, Kumar ND, Zhao CF, Prasad PN (1997) Two-photon photodynamic therapy. *J Clin Laser Med Surg* 15:201
5. Sanchez EJ, Novotny L, Xie XS (1999) Near-field fluorescence microscopy based on two-photon excitation with metal tips. *Phys Rev Lett* 82:4014
6. Gryczynski I, Malicka J, Shen Y, Gryczynski Z, Lakowicz JR (2002) Excited-state lifetime assay for protein detection on gold colloids-fluorophore complexes. *J Phys Chem B* 106:2191
7. Stellacci F, Bauer CA, Friedrichsen TM, Wenseleers W, Marder SR, Perry JW (2005) Ultrabright supramolecular beacons based on self-assembly of two-photon chromophores on metal nanoparticles. *J Am Chem Soc* 125:328
8. Cohanoschi I, Hernández FE (2005) Surface plasmon enhancement of two- and three-photon absorption of Hoechst 33258 dye in activated gold colloid solution. *J Phys Chem B* 109:14506
9. Kreibitz U, Volmer M (1995) Optical properties of metal clusters: Springer series in materials science. Springer, Berlin, Vol.25
10. Schwartzberg AM, Zhang JZ (2008) Novel optical properties and emerging applications of metal nanostructures. *J Phys Chem C* 112:10323
11. Garcia-Vidal FJ, Pendry J (1996) Collective theory for surface enhanced Raman scattering. *Phys Rev Lett* 77:1163
12. Sarychev AK, Shalaev VM (2002) Theory of nonlinear optical responses in metal–dielectric composites. *Top Appl Phys* 82:169
13. Haes AJ, Zou SL, Schatz GC, Van Duyne RP (2004) Nanoscale optical biosensor: short range distance dependence of the localized surface plasmon resonance of noble metal nanoparticles. *J Phys Chem B* 108:6961
14. Boni LD, Wood E, Toro C, Hernandez F (2008) Optical saturable absorption in gold nanoparticles. *Plasmonics* 3:171
15. Homola J, Yee S, Gauglitz G (1999) Surface plasmon resonance sensors: review. *Sens Actuators B* 54:3
16. Elghanian R, Storhoff JJ, Mucic RC, Letsinger RL, Mirkin CA (1997) Selective colorimetric detection of polynucleotides based on the distance-dependent optical properties of gold nanoparticles. *Science* 277:1078
17. Mishra YK, Mohapatra S, Avasthi DK, Kabiraj D, Lalla NP, Pivni JC, Sharma H, Kar R, Singh N (2007) Gold–silica nanocomposites for the detection of human ovarian cancer cells: a preliminary study. *Nanotechnology* 18:345606
18. Haes AJ, Van Duyne RP (2004) A unified view of propagating and localized surface plasmon resonance biosensors. *Anal Bioanal Chem* 379:920

19. Xu HX, Kall M (2002) Surface-plasmon-enhanced optical forces in silver nanoaggregates. *Phys Rev Lett* 89:246802
20. Shao DB, Chen SC (2005) Surface-plasmon-assisted nanoscale photolithography by polarized light. *Appl Phys Lett* 86:253107
21. Jensen TR, Malinsky MD, Haynes CL, Van Duyne RP (2000) Nanosphere lithography: tunable localized surface plasmon resonance spectra of silver nanoparticles. *J Phys Chem B* 104:10549
22. Palpant B, Prevel B, Lerme J, Cottancin E, Pellarin M, Treilleux M, Perez A, Vialle JL, Broyer M (1998) Optical properties of gold clusters in the size range 2–4 nm. *Phys Rev B* 57:1963
23. Wang J, Lau WM, Li Q (2005) Effects of particle size and spacing on the optical properties of gold nanocrystals in alumina. *J Appl Phys* 97:114303
24. Miotello A, De Marchi G, Mattei G, Mazzoldi P, Sada C (2001) Clustering of gold atoms in ion-implanted silica after thermal annealing in different atmospheres. *Phys Rev B* 63:075409
25. Takeda Y, Lu J, Plaksin OA, Amekura H, Kono K, Kishimoto N (2004) Optical properties of dense Cu nanoparticle composites fabricated by negative ion implantation. *Nucl Instrum Meth Phys Res B* 219–220:737
26. Karthikeyan B, Anija M, Sandeep CSS, Nadeer TMM, Philip R (2008) Optical and nonlinear optical properties of copper nanocomposite glasses annealed near the glass softening temperature. *Opt Commun* 281:2933
27. Schürmann U, Hartung WA, Takele H, Zaporozhchenko V, Faupel F (2005) Controlled syntheses of Ag–polytetrafluoroethylene nanocomposite thin films by co-sputtering from two magnetron sources. *Nanotechnology* 16:1078
28. Mohapatra S, Mishra YK, Avasthi DK, Kabiraj D, Ghatak J, Varma S (2007) Synthesis of Au nanoparticles in partially oxidized Si matrix by atom beam sputtering. *J Phys D: Appl Phys* 40:7063
29. Mohapatra S, Mishra YK, Kabiraj D, Avasthi DK, Ghatak J, Varma S (2008) Synthesis of gold-silicon core-shell nanoparticles with tunable localized surface plasmon resonance. *Appl Phys Lett* 92:103105
30. Bahae MS, Said AA, Stryland EWV (1989) High-sensitivity, single-beam n_2 measurements. *Opt Lett* 14:955
31. Doolittle LR (1985) Algorithms for the rapid simulation of Rutherford backscattering spectra. *Nucl Instrum Methods B* 9:344–351
32. Tamura A, Higeta K, Ichinokawa T (1982) Lattice vibrations and specific heat of a small particle. *J Phys C* 15:4975
33. Montagna M, Dusi R (1995) Raman scattering from small spherical particles. *Phys Rev B* 52:10080
34. Ziegler JF, Biersack JP, Littmark U (1985) The stopping and range of ions in solids. Pergamon, Oxford
35. Sutherland RL (1996) Handbook of nonlinear optics. Dekker, New York
36. Sandeep CSS, Philip R, Satheeshkumar R, Kumar V (2006) Sol-gel synthesis and nonlinear optical transmission in $Zn_{(1-x)}Mg_xO$ ($x \leq 0.2$) thin films. *Appl Phys Lett* 89:063102
37. Ambika D, Kumar V, Sandeep CSS, Philip R (2009) Non-linear optical properties of $(Pb_{1-x}Sr_x)TiO_3$ thin films. *Appl Phys B* 97:661
38. Karthikeyan B, Anija M, Philip R (2006) In situ synthesis and nonlinear optical properties of Au:Ag nanocomposite polymer films. *Appl Phys Lett* 88:053104
39. Irimpan L, Nampoorei VPN, Radhakrishnan P (2008) Spectral and nonlinear optical characteristics of nanocomposites of ZnO–Ag. *Chem Phys Lett* 455:265